

Leveraging Multiple Descriptive Features for Robust Few-shot Image Learning

Zhili Feng
Carnegie Mellon University
zhilif@andrew.cmu.edu

Anna Bair
Carnegie Mellon University
abair@cmu.edu

J. Zico Kolter
Carnegie Mellon University
zkolter@cs.cmu.edu

Abstract

Modern image classification is based upon directly predicting model classes via large discriminative networks, making it difficult to assess the intuitive visual “features” that may constitute a classification decision. At the same time, recent works in joint visual language models such as CLIP provide ways to specify natural language descriptions of image classes but typically focus on providing single descriptions for each class. In this work, we demonstrate that an alternative approach, arguably more akin to our understanding of multiple “visual features” per class, can also provide compelling performance in the robust few-shot learning setting. In particular, we automatically enumerate multiple visual descriptions of each class – via a large language model (LLM) – then use a vision-image model to translate these descriptions to a set of multiple visual features of each image; we finally use sparse logistic regression to select a relevant subset of these features to classify each image. This both provides an “intuitive” set of relevant features for each class, and in the few-shot learning setting, outperforms standard approaches such as linear probing. When combined with finetuning, we also show that the method is able to outperform existing state-of-the-art finetuning approaches on both in-distribution and out-of-distribution performance.

1. Introduction

Self-supervised vision-language models (VLMs) like CLIP [1] create aligned image and text encoders via contrastive training. Unlike traditionally-trained classification networks, such alignment enables zero-shot image classification by prompting the text encoder with hand-crafted inputs like “a photo of { }” then predicting the target via the maximal inner product with the input image embedding. However, choosing effective prompts for zero-shot learning remains largely an ad-hoc process: Radford et al. [1] has added several prompts like “the cartoon { }” or “art of the { }” aiming to improve ImageNet-R [2] performance, which (somewhat surprisingly) improving standard

ImageNet accuracy as well. This has led to works that attempt to automatically extract relevant prompts from language models [3], including work that uses these models to extract *multiple* visual descriptors [4] then use the average prediction of these visual descriptions to classify the image.

In the few-shot setting, however, where a small amount of training data is available, a number of techniques can further improve classifier performance beyond zero-shot prompting alone. For example, it has become commonplace to finetune zero-shot classifiers via linear probing or other approaches [5], including methods that interpolate between the zero-shot and finetuned classifiers [6] to achieve better out-of-distribution robustness. Alternatively, one can also adapt the prompts themselves using this few-shot data, using e.g. techniques from soft prompt tuning [7], though these learned prompts are not readable, nor are their nearest dictionary projections [8]. Finally, recent work has also looked at ways to combine automatically-extracted prompts using few-shot learning [9], though this approach used a very specific learned weighting over such descriptions, and its performance lagged behind simple linear probing for even small numbers of examples.

In this work, we propose a simple and effective method to generate classifiers based upon multiple automatically-extracted visual descriptors of each class. Specifically, we use a language model to extract multiple potential visual features of each class, then use ℓ_1 -regularized logistic regression to fit a sparse linear classifier on top of these visual descriptions. The key observation that supports our method is that the (sparsely selected) visual descriptors are able to distinguish different classes, even if the multi-modal model is not trained on such supervision explicitly, and also provide an intuitive understanding of which features are important to which classes. Once the important visual descriptors are selected, we can additionally finetune the image encoder with the selected sparse pattern to further improve classification accuracies. Our proposed method outperforms baselines on both in-distribution (ID) and out-of-distribution (OOD) image classification across a range of image datasets. Doing sparse logistic regression with visual descriptors on ImageNet and its variations outperforms lin-

ear probing with image features by 6.2% to 10.48% varying k -shot from $k = 1$ to $k = 32$. When combining our method with WISE-FT [6], on in-distribution task finetuning with a fixed sparse pattern outperform standard finetuning by 1.43% with 1-shot, 1.62% with 2-shot, and 1.61% with 4-shot training data; averaging over five ImageNet variations, we outperform standard finetuning by 0.88% with 1-shot, 0.73% with 2-shot, and 0.64% with 4-shot training data.

1.1. Notation

Throughout the paper, we use $g(\cdot)$ to denote the text encoder and $f(\cdot)$ to denote the image encoder. We use \mathbf{t} for text tokens and \mathbf{p} for images. For a vector \mathbf{v} , subscript v_i represents the i th entry. We sometimes overload the notation \mathbf{t}_c to represent a vector belonging to a class c , this should be clear from the context.

2. Related works and motivation

2.1. Prompt tuning in NLP

GPT-2 and 3 [10, 11] incited a new in-context learning paradigm of applying LLMs to downstream tasks, in which one provides a prompt to elicit a response or action, then optionally provides several demonstrations in this context. Prompt tuning has been demonstrated to be quite data efficient: Scao and Rush [12] shows that appropriate prompting is often worth hundreds of data points.

Discrete Prompt Tuning AutoPrompt [13] searches for a fixed-length prompt in a token-by-token greedy fashion. For each token position, they first select the top- k candidate tokens that align the most with the gradient of the log-likelihood, while fixing the prompts; then they select from the k candidates the one that maximizes the log-likelihood. The first step requires one forward-backward pass of the model, and the second step takes k forward steps. This greedy algorithm generates prompts that are readable but not understandable. For example, they generate the following prompts for a sentiment analysis task: “a real joy. atmosphere alot dialogue Clone totally [MASK]”. Guo et al. [14] uses Q-learning to generate prompts but still lacks comprehensibility. Gao et al. [15] leverage T5 [16] to generate prompt templates that contain the training pairs, and pick the best template based on the training data. Recently, Shi et al. [17] proposed to sample human-readable prompts based on Langevin dynamics incorporated with a fluency constraint. There are also works that suggest prompt engineering via edit-based enumeration [18], data mining [19], and even LLMs themselves [20].

Continuous Prompt Tuning Continuous prompt tuning optimizes over the continuous text embedding space, usu-

ally through gradient descent with the training data while fixing the model parameters [21, 22, 23, 24]. These approaches are usually faster and more scalable compared to discrete prompt tuning, although the searched prompts are not semantically meaningful [25, 8].

2.2. Prompt tuning in VLMs

Contrastive VLMs aim to minimize the contrastive loss between matching image-text pairs. Let the image embedding be $f(\mathbf{p}) \in \mathbb{R}^{(1+M) \times d}$, the text embedding be $g(\mathbf{t}) \in \mathbb{R}^{(1+P) \times d}$. WLOG, let the first entry of the embeddings be the [CLS] token, denote as $g(\mathbf{t})_0$. The probability of the prediction is then represented as:

$$p(y = c | \mathbf{p}, \mathbf{t}) = \frac{\exp(\langle f(\mathbf{p})_0, g(\mathbf{t}_c)_0 \rangle / \tau)}{\sum_{c'} \exp(\langle f(\mathbf{p})_0, g(\mathbf{t}_{c'})_0 \rangle / \tau)},$$

where \mathbf{t}_c is the zero-shot text prompt for class c . The class whose prompt has the largest inner product with the image embedding will be the zero-shot prediction. Zhou et al. [7] optimizes over the embedding space of x_T for the best prompts. Several follow-up works [26, 27] propose various prompt tuning methods for different task settings. The methods that eventually use $g(\mathbf{t}_c)_0$ are in essence regularized linear probing in the sense that the search space is constrained by the co-domain of $g(\cdot)_0$. Chen et al. [28] uses local information of the image embedding f_1, \dots, f_{M+1} for optimizing an optimal transport distance between local image information and prompts. Lu et al. [29] learns distributions over prompts for efficient adaptation to downstream recognition tasks. Wen et al. [30] discusses discrete prompt search in the context of text-to-image settings.

Pratt et al. [3] prompts LLMs for descriptions of each class and shows that these prompts can achieve better zero-shot image classification accuracy. Menon and Vondrick [4] prompt LLMs to generate visual descriptors for image classification. For each class c , they query GPT-3 using the prompt “What are useful features for distinguishing a $\{c\}$ in a photo?”. A score is estimated for c given an image x :

$$s(c, x) = \frac{1}{|D(c)|} \sum_{d \in D(c)} \phi(d, x),$$

where $D(c)$ is the number of descriptors for c , and $\phi(d, x) = \langle \text{Encode}(d), \text{Encode}(x) \rangle$ is the grounding between the image and text features. They show this average ensemble can outperform zero-shot classifiers while maintaining interpretability.

Similar to what we propose, LaBo [9] also considers per-class level descriptions in the few-shot setting. A key difference is that they perform a per-class level description filtering through submodular optimization, and they use a

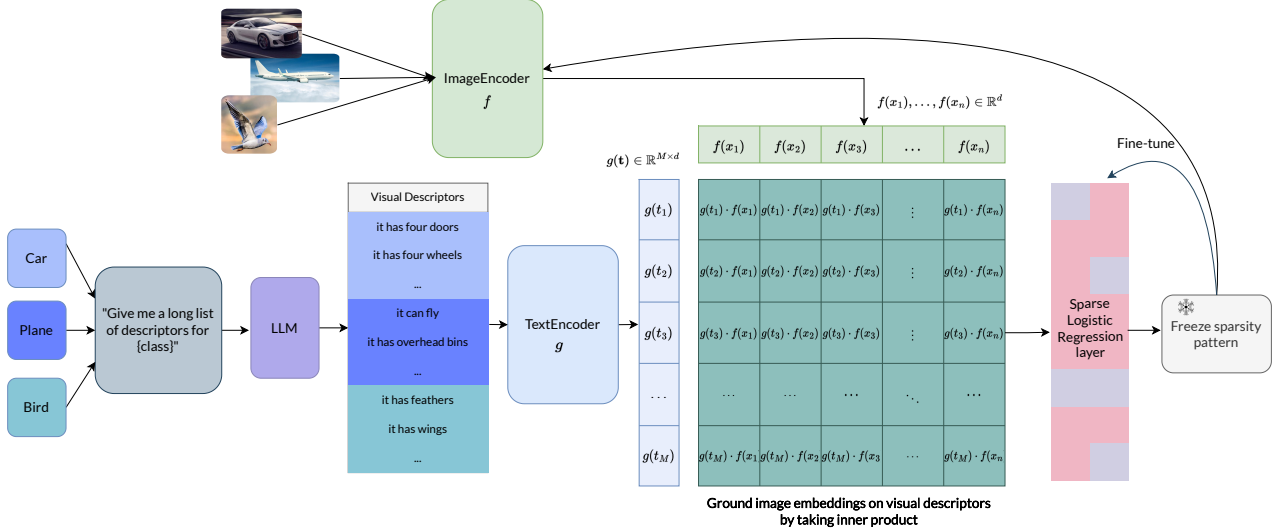


Figure 1: An overview of our proposed method. We prompt GPT-3 for a list of visual descriptors for each class and encode these texts. The image embeddings are grounded to these descriptors by taking inner products. For an image embedding in \mathbb{R}^d , this operation projects it onto a \mathbb{R}^M dimensional space, but it may live in a submanifold. We apply sparse logistic regression over all $\mathbb{R}^n \times \mathbb{R}^M$ training data for feature selection. Finally, we **freeze** the sparsity pattern and finetune both the linear layer and the image encoder to align the image features with the visual descriptors.

softmax-ed linear weight $\sigma(\mathbf{W})$ to ensemble the selected features. On the other hand, we directly select features using sparse logistic regression. Our approach immediately gives both the important features and the coefficients and is statistically optimal under certain sparsity assumptions. One of the potential drawbacks of LaBo is their visual descriptions are filtered per-class level, which can hinder feature sharing between classes. This partly explains why on ImageNet LaBo starts to underperform linear probing when $k \geq 4$ (see Figure 3. in their paper). Since they focus on interpretability, LaBo enforces $\sigma(\mathbf{W})$ for a probabilistic interpretation, whereas we focus on robustness and only require \mathbf{W} to be sparse.

2.3. Robust fine-tuning of zero-shot models

There are numerous works that discuss fine-tuning zero-shot models robustly [31, 5, 6], in this work we adopt WISE-FT introduced by Wortsman et al. [6] to improve the out-of-distribution accuracy.

Let the finetuned weight be Φ_{learned} and let the zero-shot predictor be Φ_{zs} . Wortsman et al. [6] observes that while Φ_{learned} performs better than Φ_{zs} on in-distribution tasks, it is worse at out-of-distribution tasks. Hence they propose to interpolate the two sets of weights as $\alpha \Phi_{\text{learned}} + (1 - \alpha) \Phi_{\text{zs}}$. This surprisingly simple weight ensemble help both in-distribution and out-of-distribution tasks. This method also naturally applies to linear probing by simply freezing the CLIP encoder throughout, and only training and interpolat-

ing the linear head.

2.4. Motivation and observation

Contrastive training allows CLIP for zero-shot classification via the usage of prompts like “a photo of {label}”. Can we also reason about the class of images with more detailed semantic features like “it has fur” or “it has a snout”? This kind of reasoning not only tells us to which class the image belongs but also *why* it belongs to the class. Arguably using multiple descriptive features to classify images is also more intuitive and interpretable to humans. Besides interpretability, are there other benefits of these descriptive features?

Surprisingly, we find that even if the contrastive learning process does not explicitly tell the model why the image belongs to a certain class, the semantic differences between classes are still preserved in the image embedding space. Some of the semantic differences can even be abstract ideas that are unlikely to be visually discerned from the image. We illustrate this phenomenon with the following example. We randomly sample 500 plane images and 500 car images from the CIFAR-10 dataset, and compute their cosine similarity with 5 prompts:

1. “it has wings”
2. “it has four doors”
3. “a photo of an airplane”
4. “a photo of an automobile”

5. “it is lethal to crash”

The cosine similarities are plotted in fig. 2. There are clear separations between classes using these prompts, even if the contrastive training does not necessarily associate prompts 1, 2, and 5 with the image themselves. A particularly interesting prompt is “it is lethal to crash”, as its intuition may not matches with that of humans that plane crashes are more dangerous than car accidents, which suggests that not all seemingly intuitive prompts can be applied in the zero-shot setting. Even if prompts 1, 2, and 5 are weaker separators compared to prompts 3 and 4, this observation leaves us with the possibility to ensemble many weak features for a good classifier.

3. Proposed method

In this section, we present our proposed method, fig. 1 provides an overview. We will discuss how to generate features, select a sparse set of useful descriptions, and finally, how to align the encoder in detail.

3.1. Generate visual descriptors

To generate the visual descriptors for ImageNet and its variations, we first use the following prompt to query GPT-3: “Give me a long list of descriptions for {label}:”.

GPT-3 is quite sensitive to format instruction. Using the prompt “Give me a list” always leads to a list format, making it straightforward to select the useful text with regular expressions. We also did not explicitly ask GPT-3 for visual features. As we have shown in section 2.4, even abstract text can be used for classification. Following the method in Menon and Vondrick [4], we condition these descriptors on the class name, using texts of the form “{c} which has {t_cⁱ” for each class *c* and the *i*th descriptor. For each class *c*, we gather *M_c* descriptors from GPT-3.

Furthermore, for each class, there exists a set of hand-crafted prompt templates like “a photo of { }” or “an art of { }”. If there are *T* total number of such templates, using the class name *c*, we can generate *T* total prompt embeddings for each class. We take the average of these prompt embeddings *in addition* to the aforementioned visual descriptors, leading to *M_c* + 1 number of prompts for each class. For simplicity, we will refer to the GPT-3 generated text features as *visual descriptors (VD)*, the templates with class names as *class prompts*, and the union as *augmented visual descriptors (AVD)*. We will also refer to their *embeddings* using the same names, which should be clear from the context.

Denote $M = \sum_{c \in \mathcal{C}} M_c$. The visual descriptors, class prompts, and augmented visual descriptors can be encoded into three matrices $\mathbf{U}_{\text{vd}} \in \mathbb{R}^{M \times d}$, $\mathbf{U}_{\text{cp}} \in \mathbb{R}^{|\mathcal{C}| \times d}$, $\mathbf{U}_{\text{avd}} \in \mathbb{R}^{(M+|\mathcal{C}|) \times d}$. Given an image embedding $\mathbf{z} := f(\mathbf{p})_0 \in$

\mathbb{R}^d , these three matrices respectively created three sets of groundings $\mathbf{h}_{\text{vd}} = \mathbf{U}_{\text{vd}}\mathbf{z}$, $\mathbf{h}_{\text{cp}} = \mathbf{U}_{\text{cp}}\mathbf{z}$, and $\mathbf{h}_{\text{avd}} = \mathbf{U}_{\text{avd}}\mathbf{z}$. Notice that all three \mathbf{U} matrices are fixed and never trained. With the grounded features \mathbf{h} , we can learn three matrices $\mathbf{W}_{\text{vd}} \in \mathbb{R}^{|\mathcal{C}| \times M}$, $\mathbf{W}_{\text{cp}} \in \mathbb{R}^{|\mathcal{C}| \times |\mathcal{C}|}$, $\mathbf{W}_{\text{avd}} \in \mathbb{R}^{|\mathcal{C}| \times (M+|\mathcal{C}|)}$.

Setting

$$\mathbf{W}_{\text{vd}} = \text{blkdiag} \left(\underbrace{\left\{ \frac{1}{M_c}, \dots, \frac{1}{M_c} \right\}}_{|M_c| \text{ copies}} \right)_{c \in \mathcal{C}},$$

then $\mathbf{W}_{\text{vd}}\mathbf{U}_{\text{vd}}$ leads to the average ensemble in Menon and Vondrick [4]. Setting $\mathbf{W}_{\text{cp}} = I_{|\mathcal{C}| \times |\mathcal{C}|}$, we get back the zero-shot classifier $\mathbf{W}_{\text{zs}} = \mathbf{W}_{\text{cp}}\mathbf{U}_{\text{cp}}$. One can naturally merge \mathbf{W}_{vd} and \mathbf{W}_{cp} into $\mathbf{W}_{\text{avd}} = [\mathbf{W}_{\text{vd}}, \mathbf{W}_{\text{cp}}]$. Notice these three matrices can all serve as zero-shot classifiers.

3.2. Learning sparse visual descriptors ensemble

The previously defined matrix \mathbf{U}_{avd} can be viewed as a linear projection of the image embedding onto a $M + |\mathcal{C}|$ dimensional semantic space. While this space has a high ambient dimension, the projected embeddings live in a low-dimensional manifold that has rank less than or equal to that of the image embedding space. By enforcing a sparsity constraint on \mathbf{W}_{avd} , we can select the most important dimensions among \mathbf{U}_{avd} . We demonstrate that the selected subspace is also robust to natural distribution shifts. Intuitively, we imagine that the large distribution shift in the image embedding space only corresponds to a small shift in the semantic space, since the semantics of images should be invariant. Further investigation on the property of the semantic space is left to future works.

With a fixed \mathbf{U}_{avd} , we learn \mathbf{W}_{avd} with ℓ_1 regularization $\|\mathbf{W}_{\text{avd}}\|_1$. Not only does sparse logistic regression select the important features, but it actually also finds the intuitive features. On CIFAR-10, we demonstrate that the selected features are usually the ones that actually describe that class. For each class, we pick the 3 features with the largest coefficients. The results are listed in table 2.

3.3. Aligning the image encoder

After obtaining a sparse $\widehat{\mathbf{W}}_{\text{avd}}$, we fix \mathbf{U}_{avd} and the *sparsity pattern* of $\widehat{\mathbf{W}}_{\text{avd}}$, and finetune both the image encoder *f*, as well as the entries in $\widehat{\mathbf{W}}_{\text{avd}}$. This process aligns with LP-FT [5], which theoretically justifies its improvement in robustness.

4. Experiment

Throughout the experiments, we focus on the few-shot setting. We test our method on ImageNet, ImageNet-R, ImageNet-V2, ImageNet-A, ImageNet-Sketch, and Ob-

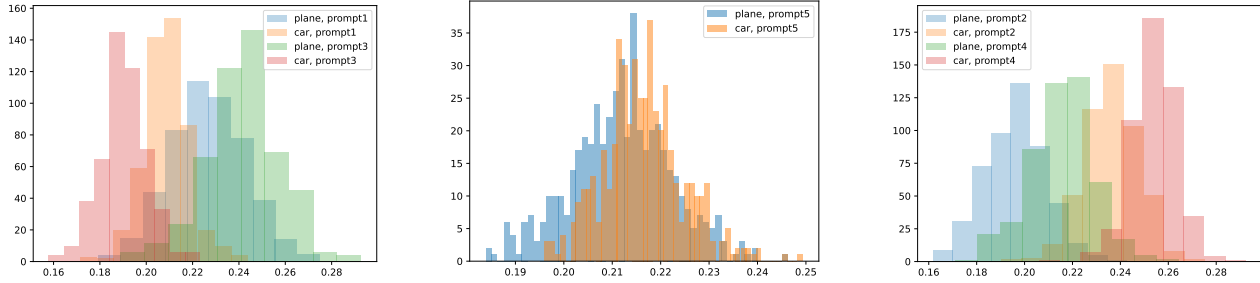


Figure 2: The cosine similarity between 500 car images, 500 plane images from CIFAR-10, and 4 prompts. **Prompt1**: “it has wings”. **Prompt2**: “it has four doors”. **Prompt3**: “a photo of an airplane”. **Prompt4**: “a photo of an automobile”. **Prompt5**: “it is lethal to crash”. We see that even though the training process may not explicitly associate plane or car images with prompt1, prompt2, and prompt5, they still separate the data well.

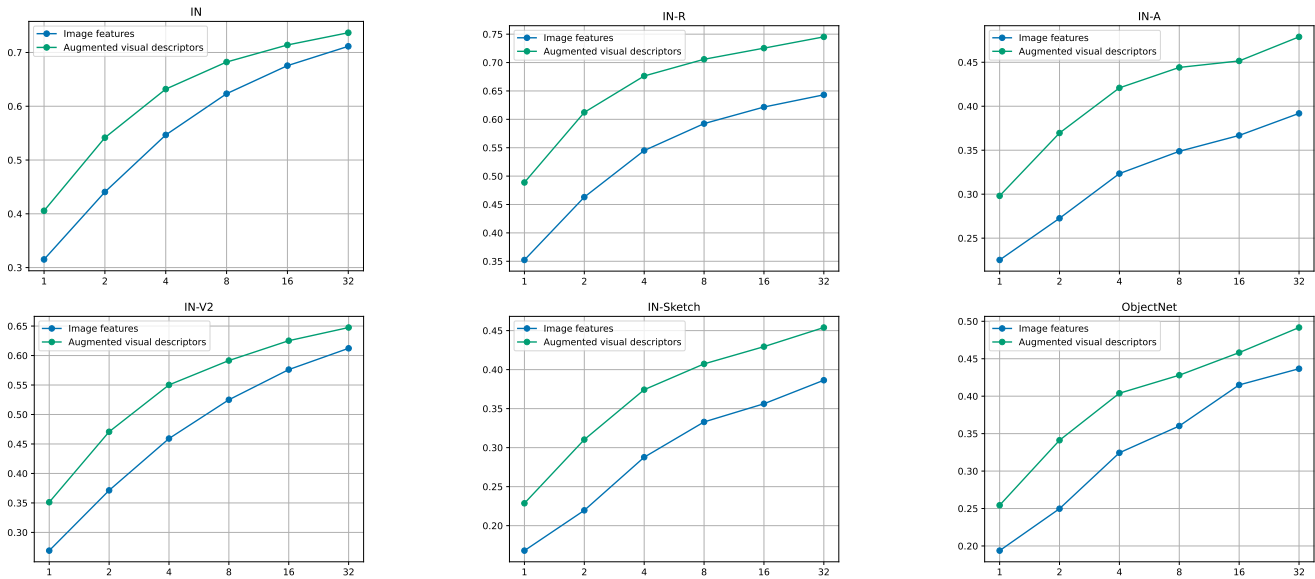


Figure 3: Few-shot experiments compare LP vs SLR-AVD. In each subfigure, the y-axis represents the number of shots per class. Here we consider shot in [1, 2, 4, 8, 16, 32] per class. SLR-AVD is more sample efficient in the in-distribution reference and is also much more robust to several distribution shifts.

jectNet [32, 2, 33, 34, 35, 36], demonstrating the superiority of the learned ensemble over visual descriptors. By default, we use the ViT-B/16 model unless otherwise specified. The hand-crafted templates for ImageNet classes contain a set of seven prompts suggested in <https://github.com/openai/CLIP>:

1. “itap of a {}.”
2. “a bad photo of the {}.”
3. “a origami {}.”
4. “a photo of the large {}.”
5. “a {} in a video game.”
6. “art of the {}.”

7. “a photo of the small {}.”

This set usually outperforms the original 80 templates in Radford et al. [1].

For simplicity, we will use the following acronyms for different methods and datasets.

ZS: Zero-shot classification using text embeddings of hand-crafted prompts ensembles. **ZS-VD**, **ZS-AVD**: Zero-shot classification using visual descriptor and augmented visual descriptors, respectively. **LP**: Linear probing using image embeddings. **SLR-AVD**: Sparse logistic regression using AVDs. **FT**: Finetuning the image encoder and classification head. **SLR-FT-AVD**: Sparse logistic regression with AVD, and then finetune the linear head plus the image encoder with frozen sparsity patterns. **WISE-FT**: Weight ensemble

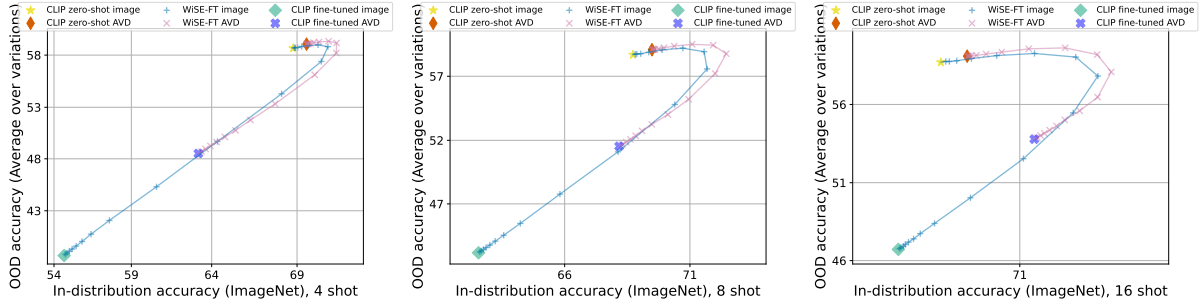


Figure 4: ID-OOD accuracy curve of weight ensemble of LP vs weight ensemble of SLR-AVD. ID is tested on ImageNet, and OOD is averaged over 5 ImageNet variations. Experiments with [4, 8, 16]-shots are presented. Each accuracy is averaged over 3 runs. We can see that our proposed method overwhelms LP in all cases.

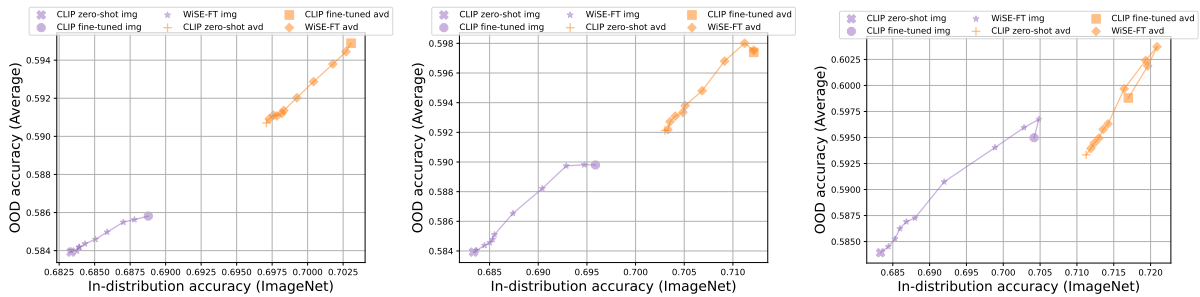


Figure 5: ID-OOD accuracy curve of WISE-FT vs WISE-SLR. ID is tested on ImageNet, and OOD is averaged over 5 ImageNet variations. Experiments with [1, 2, 4]-shots are presented. Each accuracy is averaged over 3 runs. We can see that our proposed method overwhelms WISE-FT in all cases.

	ZS	ZS-VD	ZS-AVD
IN	68.78	65.89	69.52
IN-V2	62.23	59.19	62.97
IN-R	77.72	72.75	77.85
IN-A	50.64	46.11	50.87
IN-Sketch	48.38	44.84	48.91
ObjectNet	54.31	49.60	54.58

Table 1: Accuracies of zero-shot, visual descriptors, and augmented visual descriptors on ImageNet and its variation. ZS-AVD outperforms all baselines across different datasets.

ble using ZS and FT. **WISE-SLR**: Weight ensemble using SLR-FT-AVD and ZS-AVD.

IN: ImageNet. **IN-R**: ImageNet-R. **IN-A**: ImageNet-A. **IN-V2**: ImageNetV2. **IN-Sketch**: ImageNet-Sketch.

Hyperparameter For ImageNet and its variations, we fix a set of 6804 augmented visual descriptors. The hyperparameters are swept over disjoint training and validation sets of size 20 per class for LP and SLR-AVD. For ℓ_1 regularization, its non-smoothness makes it notoriously hard for auto-

differentiation. To circumvent the smoothness issue, we apply the GPU implementation [37] of a variance-reduction proximal gradient method SAGA [38]. We adopt the *regularization path* approach, in which the solver optimizes over 100 regularization strengths $\lambda_1 > \lambda_2 \dots > \lambda_{100}$. Here we set λ_1 to be the strength that returns a model that uses none of the features, and $\lambda_{100} = 0.1 \times \lambda_1$. For LP, we always use ℓ_2 regularization, we use L-BFGS implemented by scikit-learn, and search for the regularization strength over 100 grids between 0.5 and 6. All the λ s are evenly spread in the log-space¹. For FT and SLR-FT-AVD, we select hyperparameters using a training and validation set of size 4 per class. The batch size is fixed to be 512 and the number of epochs is fixed to be 10. We always optimize with AdamW, and choose a cosine rate scheduler with warm-ups. We randomly select learning rate in $[1e-8, 3e-5]$, weight decay in $[0.1, 0.12]$, and warm up steps in $\{0, 50, 500\}$, for 20 trials. The chosen parameters are then fixed throughout all experiments.

¹In python `numpy.logspace(math.log10(λ_1), math.log10(λ_{100}), 100)`

Classes	Features
airplanes	airplanes which has anticollision lights a photo of airplanes airplanes which has overhead storage bins
cars	cars which has body kit cars which has bumpers cars which has wheel arch trim
birds	birds which has leg color birds which has flight silhouette birds which has eye color
cats	cats which has pink tongue cats which has pink nose cats which has slit pupils
deer	deer which has large facial glands deer which has long, tufted hair on the neck and shoulders deer which has short, curved antlers
dogs	dogs which has silky fur dogs which has pattern dogs which has floppy ears
frogs	frogs which has large, bulging eyes frogs which has ridged or wartylooking skin frogs which has a fold of skin along the back
horses	horses which has hooves horses which has temperament horses which has intelligence
ships	ships which has lifeboats ships which has bridge ships which has bow
trucks	trucks which has trailersway control trucks which has grille trucks which has lift kits

Table 2: Features selected when trained with ℓ_1 norm on CIFAR-10. The selected important features for each class are intuitive. Notice that the feature selection method does not restrict the candidates to be that particular class’s descriptors.

4.1. Zero-shot with AVDs

As mentioned in section 3.1, we can easily establish zero-shot matrices with AVDs. We set \mathbf{W}_{vd} to be the aforementioned block diagonal form, \mathbf{W}_{cp} to be an identity matrix. We merge them into $\mathbf{W}_{avd} = [\mathbf{W}_{vd}, \gamma \mathbf{W}_{cp}]$. Their performances are compared in table 1. ZS-AVD outperforms every zero-shot baseline on all ImageNet variations. We find that simply using VD usually underperforms ZS, indicating that the class names are probably one of the strongest prompts. This observation is intuitive as during contrastive training, the class name itself is likely to show up in the caption the most often, compared to other visual descriptors. One can certainly try to improve ZS-VD results by more carefully prompting GPT-3, or gathering descriptors from different data sources/search engines. Pratt et al. [3], Yang et al. [9], Menon and Vondrick [4] have studied the quality of descriptors across different datasets and hyperparameter

(e.g. temperature for sampling, etc) settings. Here we did not further pursue that path. Instead, we realize that simply using the merged prompts \mathbf{W}_{avd} already surpasses the best zero-shot classifier. Notice here we have a parameter γ that decides how important we weigh the zero-shot model. Empirically we find that setting $\gamma = 5$ is sufficient for all datasets.

4.2. Comparison to linear probing

We compare SLR-AVD to LP with shot [1, 2, 4, 8, 16, 32] per class. Each experiment is conducted 3 times with independent random seeds. We report the averaged test accuracy on ImageNet and its distribution shift variations, see fig. 3 for details. Our proposed method outperforms linear probing on all tasks. Detailed accuracies are presented in table 3. In a nutshell, our method outperforms linear probing by 8.39%, 10.48%, 9.52%, 7.94%, 6.54%, 6.20% on $k = 1, 2, 4, 8, 16, 32$ respectively.

Although learning with visual descriptors significantly outperforms linear probing in the few-shot setting, we should remark that ImageNet and its variations are usually considered “in-distribution” to the CLIP training data. In this case, the zero-shot model itself is usually a very strong baseline, and they typically outperform these few-shot models, as one can compare table 1 and table 3. WISE-FT serves as a strong method to improve both in-distribution and out-of-distribution accuracies. In particular, we can train a linear head $\mathbf{W}_{learned}$, and interpolate with the zero-shot weight \mathbf{W}_{zs} by taking a convex combination $\alpha \mathbf{W}_{learned} + (1 - \alpha) \mathbf{W}_{zs}$, for $\alpha = \{\alpha_1, \dots, \alpha_n\}$. We are free to vary α . Then for each α_i , we can plot that weight ensemble’s in-distribution and out-of-distribution test accuracy. This procedure thus creates an ID-OOD frontier and along the curve, some ensemble excels at both ID and OOD distribution. We further show that with WISE-FT, our method still dominates the WISE-FT with image features. See the ID-OOD curves in fig. 4. We show the plot of $k = 4, 8, 16$. SLR-AVD’s ID-OOD curve overwhelms that of LP, indicating that SLR-AVD is better at both ID and OOD tasks.

4.3. Comparison to finetuning

We compare WISE-FT the whole image encoder to WISE-SLR. The ID-OOD frontier is presented in fig. 5 and the accuracies are reported in table 4.

On in-distribution task, WISE-SLR outperforms vanilla WISE-FT by 1.43%, 1.62%, and 1.61% respectively with $k = 1, 2, 4$ training data. Averaging over 5 distribution shift datasets, with optimal α , WISE-SLR outperforms vanilla WISE-FT by 0.88%, 0.73%, and 0.64% respectively with $k = 1, 2, 4$. The optimal α is picked independently for each method on each dataset.

Shots	$k = 1$		$k = 2$		$k = 4$		$k = 8$		$k = 16$		$k = 32$	
Methods	LP	AVD	LP	AVD	LP	AVD	LP	AVD	LP	AVD	LP	AVD
IN	31.51	40.56	44.06	54.16	54.66	63.19	62.33	68.23	67.55	71.40	71.15	73.67
IN-R	35.23	48.88	46.30	61.23	54.50	67.64	59.25	70.58	62.16	72.54	64.32	74.53
IN-A	22.52	29.81	27.26	36.96	32.34	42.09	34.88	44.41	36.68	45.15	39.19	47.89
IN-V2	26.91	35.12	37.13	47.07	45.92	55.02	52.50	59.15	57.62	62.52	61.23	64.75
IN-Sketch	16.80	22.87	21.96	31.03	28.77	37.43	33.29	40.73	35.62	42.94	38.64	45.39
ObjectNet	19.38	25.43	24.98	34.11	32.44	40.39	36.02	42.80	41.50	45.82	43.67	49.17
Average \uparrow	8.39		10.48		9.52		7.94		6.54		6.20	

Table 3: Accuracies on ImageNet and its variation. We compare LP vs SLR-AVD.

Shot	$k = 1$		$k = 2$		$k = 4$	
Method	FT	SLR	FT	SLR	FT	SLR
IN	68.88	70.31	69.59	71.21	70.48	72.09
Average \uparrow	1.43		1.62		1.61	
IN-R	77.82	78.29	78.13	78.53	78.32	78.59
IN-A	50.09	51.29	50.43	51.51	52.11	52.64
IN-V2	62.32	63.74	63.07	64.37	63.50	65.30
IN-Sketch	48.45	49.35	48.75	49.63	48.99	49.92
ObjectNet	54.52	54.94	55.01	54.99	55.77	55.41
Average \uparrow	0.88		0.73		0.64	

Table 4: Accuracies on ImageNet and its variation with the optimal choice of α . We compare WISE-FT to WISE-SLR.

4.4. Comparison to CoOp

We compare linear probing with AVD to CoOp [7] as well. CoOp learns the prefix of “[prefix] classname” in the continuous token embedding space. The benefit of CoOp is that it operates in a continuous space, hence one can optimize using standard backpropagation, and it is quite sample efficient. On the other hand, due to the requirement of backprop, CoOp stores a large computation graph, hence memory-efficiency is a big advantage of SLR-AVD over CoOp.

When implementing CoOp, we choose a prefix of length 16 and do not use a suffix. The prefix is fixed for all classes. We train with Adam for 20 epochs, setting the batch size to 512. This gives us comparable results to those of the original paper.

Since CoOp injects “classname” to the prompt during inference directly, this enforces a very strong prior. For a fair comparison, we also inject a strong prior by interpolating our learned linear head $\alpha \mathbf{W}_{\text{avd}} + (1 - \alpha) \mathbf{W}_{\text{zs}}$ with the zero-shot linear classifier. We use $\alpha = 0.05k$ where k is the number of shots. Resnet-50 vision backbone is used for both methods. See the result in table 5. SLR-AVD exceeds CoOp by 1.73, 1.49, 1.55, 1.53, 1.95 on $k = 1, 2, 4, 8, 16$,

respectively.

Shots	1	2	4	8	16
CoOp	59.54	60.23	60.97	62.20	63.02
AVD	61.27	61.72	62.52	63.73	64.97
Δ	+1.73	+1.49	+1.55	+1.53	+1.95

Table 5: Accuracies of CoOp and SLR-AVD on ImageNet. For SLR-AVD, we interpolate the learned weights with zero-shot weights by $\alpha \mathbf{W}_{\text{avd}} + (1 - \alpha) \mathbf{W}_{\text{zs}}$, where $\alpha = 0.05k$ and k is the number of shot per class.

5. Conclusion

We present how to leverage descriptive features for image learning in the few-shot setting robustly. These descriptive features can be easily obtained from LLMs. Applying sparse logistic regression then successfully selects the important features, which turn out to be intuitive. Our proposed method outperforms linear probing and standard fine-tuning in both ID and OOD tasks, with or without combining with WISE-FT. This approach helps us further understand the CLIP embedding space and how the semantics serve as a strong robust prior. Moving forward, it is important to understand and quantify the robustness of the visual descriptors’ space and compare it to the image embedding space statistically. From the practical side, this work aligns image encoders to a fixed text encoder, it is valuable to study how to simultaneously align both encoders in a robust way.

References

- [1] Alec Radford, Jong Wook Kim, Chris Hallacy, Aditya Ramesh, Gabriel Goh, Sandhini Agarwal, Girish Sastry, Amanda Askell, Pamela Mishkin, Jack Clark, et al. Learning transferable visual models from natural language supervision. In *International Conference on Machine Learning*, pages 8748–8763. PMLR, 2021. [1](#), [5](#)
- [2] Dan Hendrycks, Steven Basart, Norman Mu, Saurav Kadavath, Frank Wang, Evan Dorundo, Rahul Desai, Tyler Zhu, Samyak Parajuli, Mike Guo, et al. The many faces of robustness: A critical analysis of out-of-distribution generalization. In *Proceedings of the IEEE/CVF International Conference on Computer Vision*, pages 8340–8349, 2021. [1](#), [5](#)
- [3] Sarah Pratt, Rosanne Liu, and Ali Farhadi. What does a platypus look like? generating customized prompts for zero-shot image classification. *arXiv preprint arXiv:2209.03320*, 2022. [1](#), [2](#), [7](#)
- [4] Sachit Menon and Carl Vondrick. Visual classification via description from large language models. *arXiv preprint arXiv:2210.07183*, 2022. [1](#), [2](#), [4](#), [7](#)
- [5] Ananya Kumar, Aditi Raghunathan, Robbie Jones, Tengyu Ma, and Percy Liang. Fine-tuning can distort pretrained features and underperform out-of-distribution. *arXiv preprint arXiv:2202.10054*, 2022. [1](#), [3](#), [4](#)
- [6] Mitchell Wortsman, Gabriel Ilharco, Jong Wook Kim, Mike Li, Simon Kornblith, Rebecca Roelofs, Raphael Gontijo Lopes, Hannaneh Hajishirzi, Ali Farhadi, Hongseok Namkoong, et al. Robust fine-tuning of zero-shot models. In *Proceedings of the IEEE/CVF Conference on Computer Vision and Pattern Recognition*, pages 7959–7971, 2022. [1](#), [2](#), [3](#)
- [7] Kaiyang Zhou, Jingkang Yang, Chen Change Loy, and Ziwei Liu. Learning to prompt for vision-language models. *International Journal of Computer Vision*, 130(9):2337–2348, 2022. [1](#), [2](#), [8](#)
- [8] Daniel Khoshdel, Shane Lyu, Sewon Min, Lianhui Qin, Kyle Richardson, Sameer Singh, Sean Welleck, Hannaneh Hajishirzi, Tushar Khot, Ashish Sabharwal, et al. Prompt waywardness: The curious case of discretized interpretation of continuous prompts. *arXiv preprint arXiv:2112.08348*, 2021. [1](#), [2](#)
- [9] Yue Yang, Artemis Panagopoulou, Shenghao Zhou, Daniel Jin, Chris Callison-Burch, and Mark Yatskar. Language in a bottle: Language model guided concept bottlenecks for interpretable image classification. *arXiv preprint arXiv:2211.11158*, 2022. [1](#), [2](#), [7](#)
- [10] Alec Radford, Jeffrey Wu, Rewon Child, David Luan, Dario Amodei, Ilya Sutskever, et al. Language models are unsupervised multitask learners. *OpenAI blog*, 1(8):9, 2019. [2](#)
- [11] Tom B Brown, Benjamin Mann, Nick Ryder, Melanie Subbiah, Jared Kaplan, Prafulla Dhariwal, Arvind Neelakantan, Pranav Shyam, Girish Sastry, Amanda Askell, et al. Language models are few-shot learners. *arXiv preprint arXiv:2005.14165*, 4, 2020. [2](#)
- [12] Teven Le Scao and Alexander M Rush. How many data points is a prompt worth? *arXiv preprint arXiv:2103.08493*, 2021. [2](#)
- [13] Taylor Shin, Yasaman Razeghi, Robert L Logan IV, Eric Wallace, and Sameer Singh. Autoprompt: Eliciting knowledge from language models with automatically generated prompts. *arXiv preprint arXiv:2010.15980*, 2020. [2](#)
- [14] Han Guo, Bowen Tan, Zhengzhong Liu, Eric P Xing, and Zhiting Hu. Text generation with efficient (soft) q-learning. *arXiv preprint arXiv:2106.07704*, 2021. [2](#)
- [15] Tianyu Gao, Adam Fisch, and Danqi Chen. Making pre-trained language models better few-shot learners. *arXiv preprint arXiv:2012.15723*, 2020. [2](#)
- [16] Adam Roberts and Colin Raffel. Exploring transfer learning with t5: the text-to-text transfer transformer. *Accessed on*, pages 23–07, 2020. [2](#)
- [17] Weijia Shi, Xiaochuang Han, Hila Gonen, Ari Holtzman, Yulia Tsvekov, and Luke Zettlemoyer. Toward human readable prompt tuning: Kubrick’s the shining is a good movie, and a good prompt too? *arXiv preprint arXiv:2212.10539*, 2022. [2](#)
- [18] Archiki Prasad, Peter Hase, Xiang Zhou, and Mohit Bansal. Grips: Gradient-free, edit-based instruction search for prompting large language models. *arXiv preprint arXiv:2203.07281*, 2022. [2](#)
- [19] Mozes van de Kar, Mengzhou Xia, Danqi Chen, and Mikel Artetxe. Don’t prompt, search! mining-based zero-shot learning with language models. *arXiv preprint arXiv:2210.14803*, 2022. [2](#)
- [20] Yongchao Zhou, Andrei Ioan Muresanu, Ziwen Han, Keiran Paster, Silviu Pitis, Harris Chan, and Jimmy Ba. Large language models are human-level prompt engineers. *arXiv preprint arXiv:2211.01910*, 2022. [2](#)
- [21] Guanghui Qin and Jason Eisner. Learning how to ask: Querying lms with mixtures of soft prompts. *arXiv preprint arXiv:2104.06599*, 2021. [2](#)
- [22] Brian Lester, Rami Al-Rfou, and Noah Constant. The power of scale for parameter-efficient prompt tuning. *arXiv preprint arXiv:2104.08691*, 2021. [2](#)
- [23] Xiao Liu, Yanan Zheng, Zhengxiao Du, Ming Ding, Yujie Qian, Zhilin Yang, and Jie Tang. Gpt understands, too. *arXiv preprint arXiv:2103.10385*, 2021. [2](#)

- [24] Ning Ding, Shengding Hu, Weilin Zhao, Yulin Chen, Zhiyuan Liu, Hai-Tao Zheng, and Maosong Sun. Open-prompt: An open-source framework for prompt-learning. *arXiv preprint arXiv:2111.01998*, 2021. 2
- [25] Karen Hambardzumyan, Hrant Khachatrian, and Jonathan May. Warp: Word-level adversarial reprogramming. *arXiv preprint arXiv:2101.00121*, 2021. 2
- [26] Kaiyang Zhou, Jingkang Yang, Chen Change Loy, and Ziwei Liu. Conditional prompt learning for vision-language models. In *Proceedings of the IEEE/CVF Conference on Computer Vision and Pattern Recognition*, pages 16816–16825, 2022. 2
- [27] Beier Zhu, Yulei Niu, Yucheng Han, Yue Wu, and Hanwang Zhang. Prompt-aligned gradient for prompt tuning. *arXiv preprint arXiv:2205.14865*, 2022. 2
- [28] Guangyi Chen, Weiran Yao, Xiangchen Song, Xinyue Li, Yongming Rao, and Kun Zhang. Prompt learning with optimal transport for vision-language models. *arXiv preprint arXiv:2210.01253*, 2022. 2
- [29] Yuning Lu, Jianzhuang Liu, Yonggang Zhang, Yajing Liu, and Xinmei Tian. Prompt distribution learning. In *Proceedings of the IEEE/CVF Conference on Computer Vision and Pattern Recognition*, pages 5206–5215, 2022. 2
- [30] Yuxin Wen, Neel Jain, John Kirchenbauer, Micah Goldblum, Jonas Geiping, and Tom Goldstein. Hard prompts made easy: Gradient-based discrete optimization for prompt tuning and discovery. *arXiv preprint arXiv:2302.03668*, 2023. 2
- [31] Sachin Goyal, Ananya Kumar, Sankalp Garg, Zico Kolter, and Aditi Raghunathan. Finetune like you pretrain: Improved finetuning of zero-shot vision models. *arXiv preprint arXiv:2212.00638*, 2022. 3
- [32] Jia Deng, Wei Dong, Richard Socher, Li-Jia Li, Kai Li, and Li Fei-Fei. Imagenet: A large-scale hierarchical image database. In *2009 IEEE conference on computer vision and pattern recognition*, pages 248–255. Ieee, 2009. 5
- [33] Dan Hendrycks, Kevin Zhao, Steven Basart, Jacob Steinhardt, and Dawn Song. Natural adversarial examples. In *Proceedings of the IEEE/CVF Conference on Computer Vision and Pattern Recognition*, pages 15262–15271, 2021. 5
- [34] Benjamin Recht, Rebecca Roelofs, Ludwig Schmidt, and Vaishal Shankar. Do imagenet classifiers generalize to imagenet? In *International conference on machine learning*, pages 5389–5400. PMLR, 2019. 5
- [35] Haohan Wang, Songwei Ge, Zachary Lipton, and Eric P Xing. Learning robust global representations by penalizing local predictive power. *Advances in Neural Information Processing Systems*, 32, 2019. 5
- [36] Andrei Barbu, David Mayo, Julian Alverio, William Luo, Christopher Wang, Dan Gutfreund, Josh Tenenbaum, and Boris Katz. Objectnet: A large-scale bias-controlled dataset for pushing the limits of object recognition models. *Advances in neural information processing systems*, 32, 2019. 5
- [37] Eric Wong, Shibani Santurkar, and Aleksander Madry. Leveraging sparse linear layers for debuggable deep networks. In *International Conference on Machine Learning*, pages 11205–11216. PMLR, 2021. 6
- [38] Aaron Defazio, Francis Bach, and Simon Lacoste-Julien. Saga: A fast incremental gradient method with support for non-strongly convex composite objectives. *Advances in neural information processing systems*, 27, 2014. 6

A. Appendix

As a recap, we use the following acronyms for different methods and datasets:

ZS: Zero-shot classification using text embeddings of hand-crafted prompts ensembles.

ZS-VD, ZS-AVD: Zero-shot classification using visual descriptor and augmented visual descriptors, respectively.

LP: Linear probing using image embeddings.

SLR-AVD: Sparse logistic regression using AVDs.

FT: Finetuning the image encoder and classification head.

SLR-FT-AVD: Sparse logistic regression with AVD, and then finetune the linear head plus the image encoder with frozen sparsity patterns.

WISE-FT: Weight ensemble using ZS and FT.

WISE-SLR: Weight ensemble using SLR-FT-AVD and ZS-AVD.

IN: ImageNet.

IN-R: ImageNet-R.

IN-A: ImageNet-A.

IN-V2: ImageNetV2.

IN-Sketch: ImageNet-Sketch.

The dataset-wise ID-OOD curves of LP vs SLR-AVD on IN-A, IN-R, IN-V2, IN-Sketch, and ObjectNet are listed in figs. 6 to 10, respectively.

The dataset-wise ID-OOD curves of WISE-FT vs WISE-SLR on IN-A, IN-R, IN-V2, IN-Sketch, and ObjectNet are listed in figs. 11 to 15, respectively.

The detailed accuracies of WISE-FT vs WISE-SLR with different choices of α are given in table 9 (ID) and table 8 (OOD). $\alpha = 0$ corresponds to zero-shot accuracy, and $\alpha = 1$ corresponds to full fine-tuned model. The results in the same setting with only the last linear layer trained are presented in table 6 (ID) and table 7 (OOD).

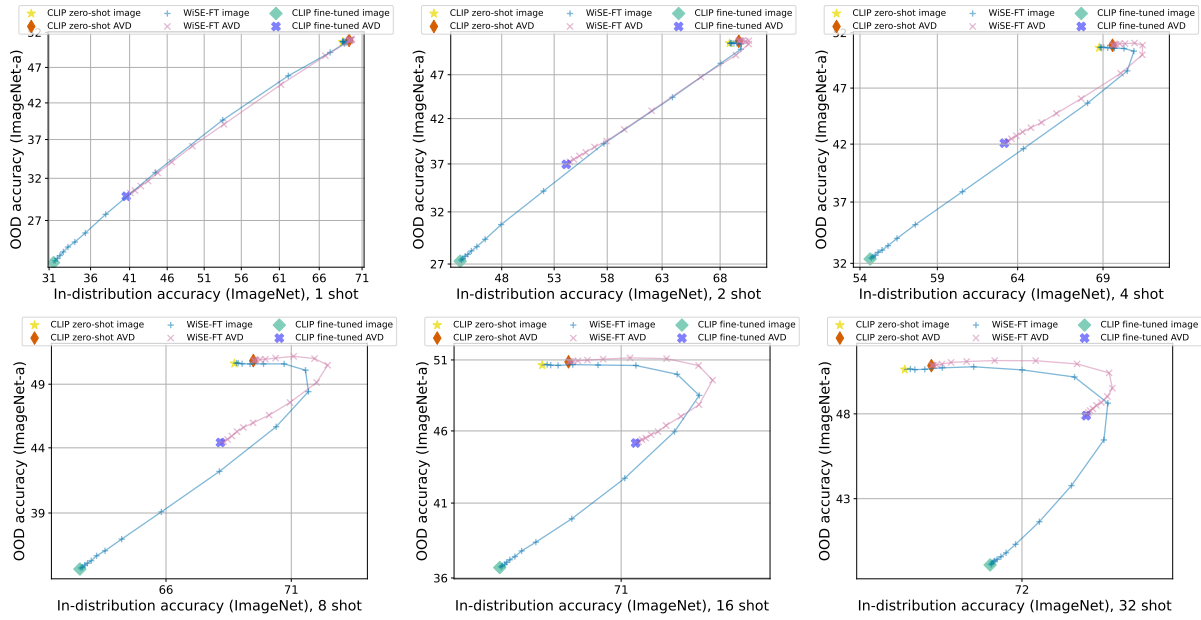


Figure 6: ID-OOD curves of LP vs SLR-AVD on IN-A. $k = 1, 2, 4, 8, 16, 32$.

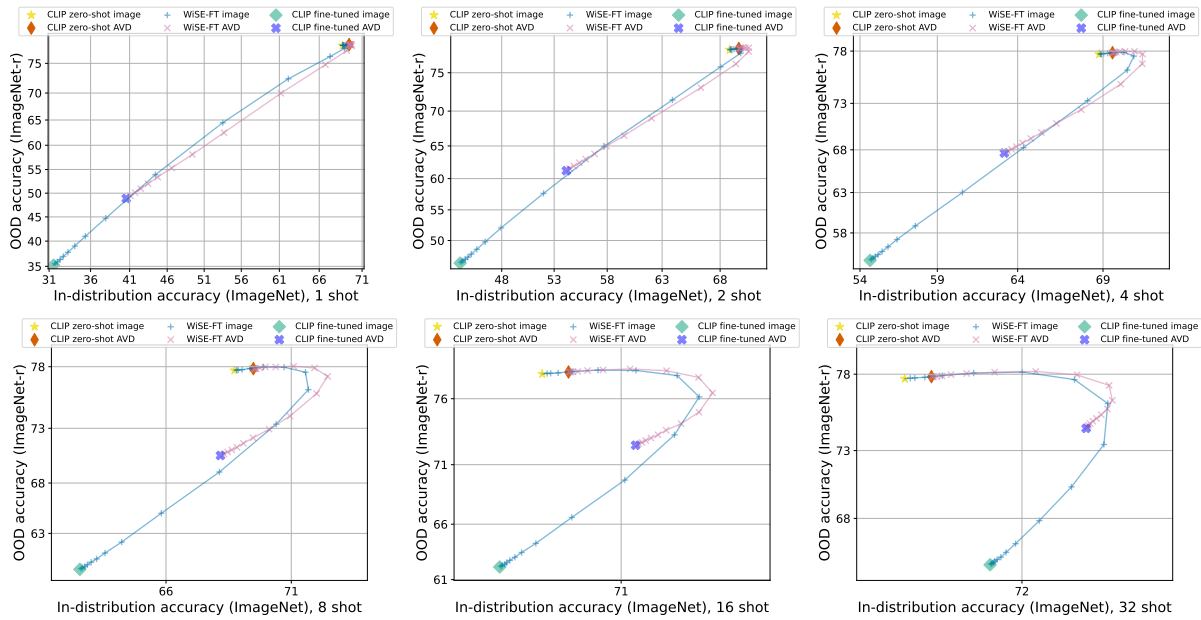


Figure 7: ID-OOD curves of LP vs SLR-AVD on IN-R. $k = 1, 2, 4, 8, 16, 32$.

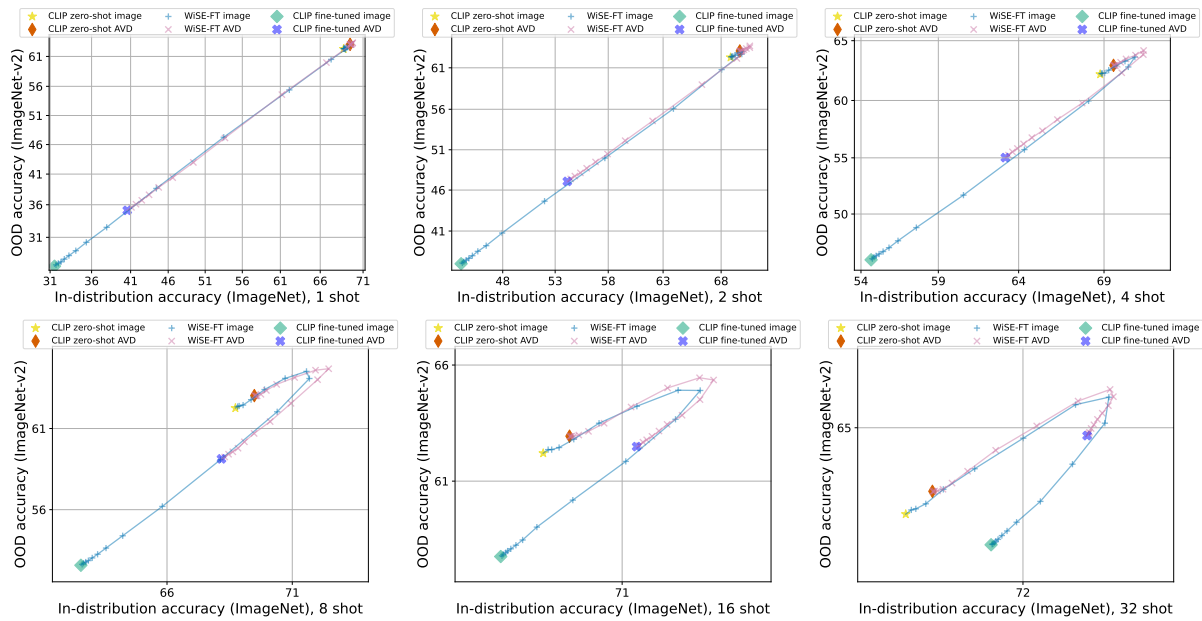


Figure 8: ID-OOD curves of LP vs SLR-AVD on IN-V2. $k = 1, 2, 4, 8, 16, 32$.

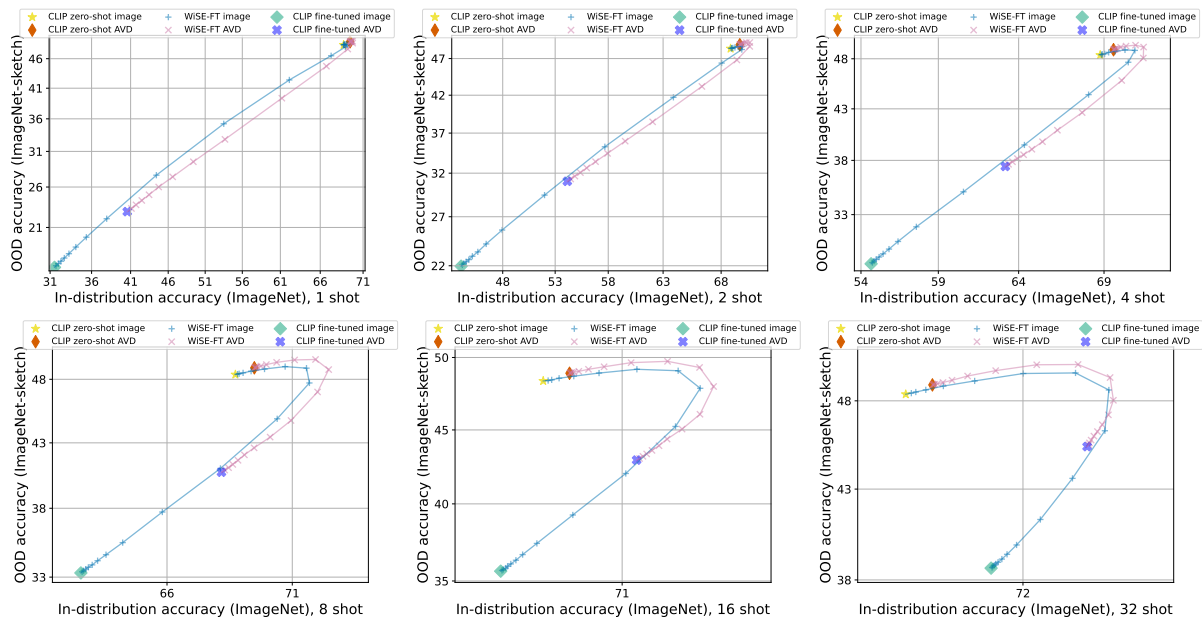


Figure 9: ID-OOD curves of LP vs SLR-AVD on IN-Sketch. $k = 1, 2, 4, 8, 16, 32$.

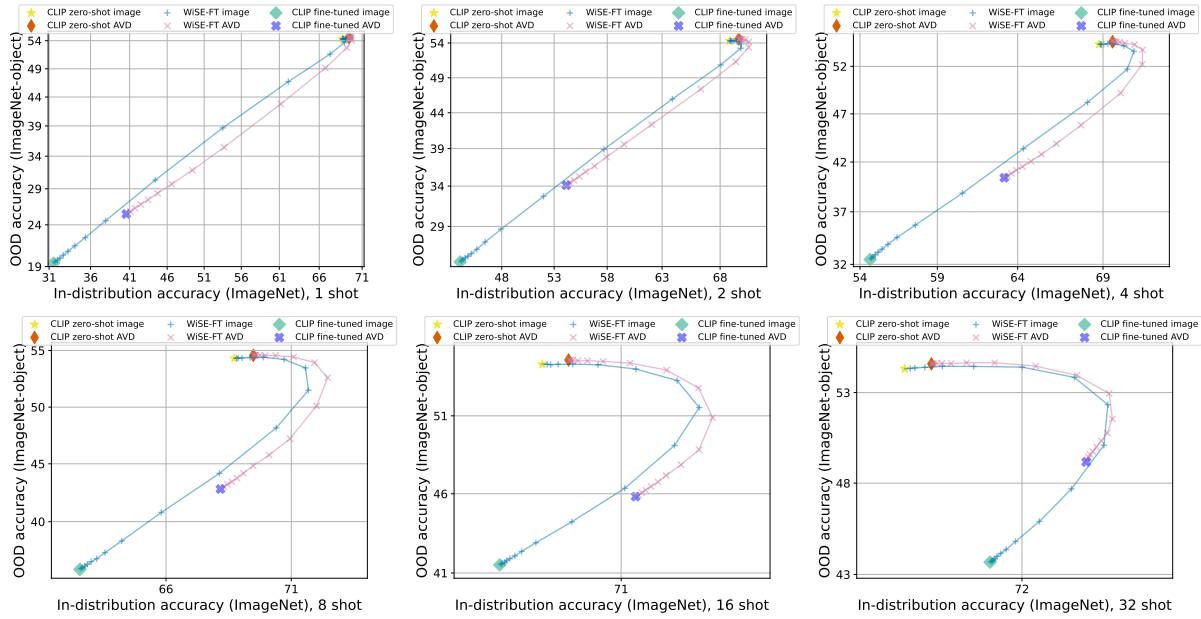


Figure 10: ID-OOD curves of LP vs SLR-AVD on ObjectNet. $k = 1, 2, 4, 8, 16, 32$.

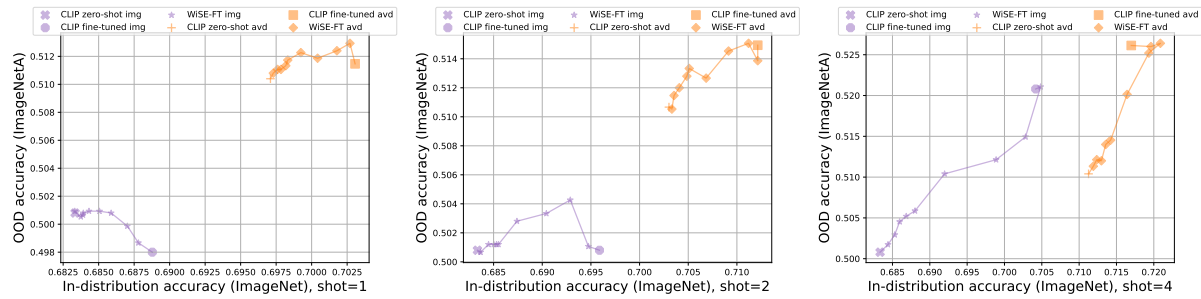


Figure 11: ID-OOD curves of WISE-FT vs WISE-SLR on IN-A. $k = 1, 2, 4$.

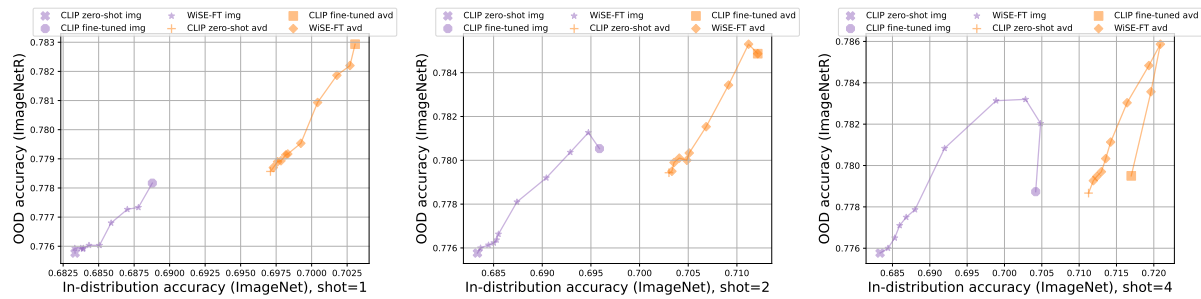


Figure 12: ID-OOD curves of WISE-FT vs WISE-SLR on IN-R. $k = 1, 2, 4$.

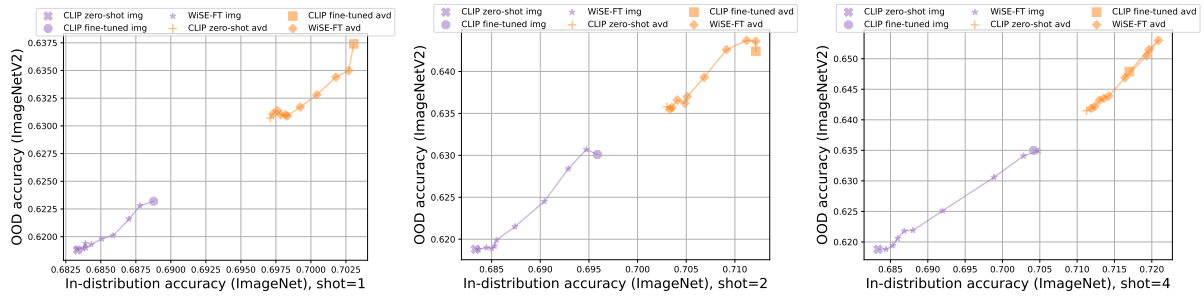


Figure 13: ID-OOD curves of WISE-FT vs WISE-SLR on IN-V2. $k = 1, 2, 4$.

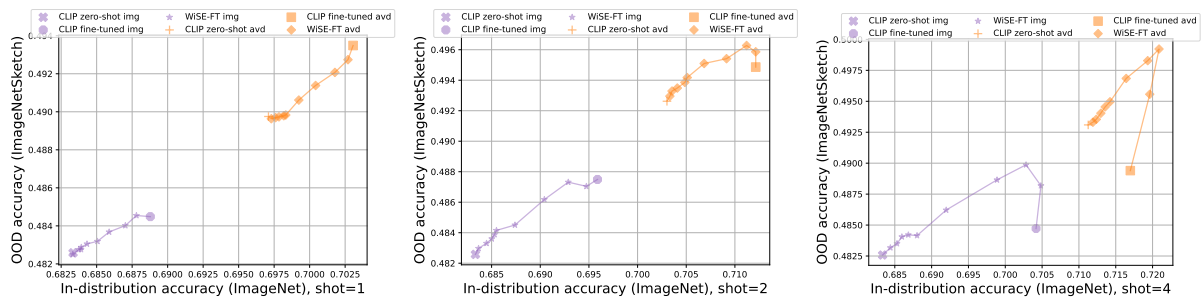


Figure 14: ID-OOD curves of WISE-FT vs WISE-SLR on IN-Sketch. $k = 1, 2, 4$.

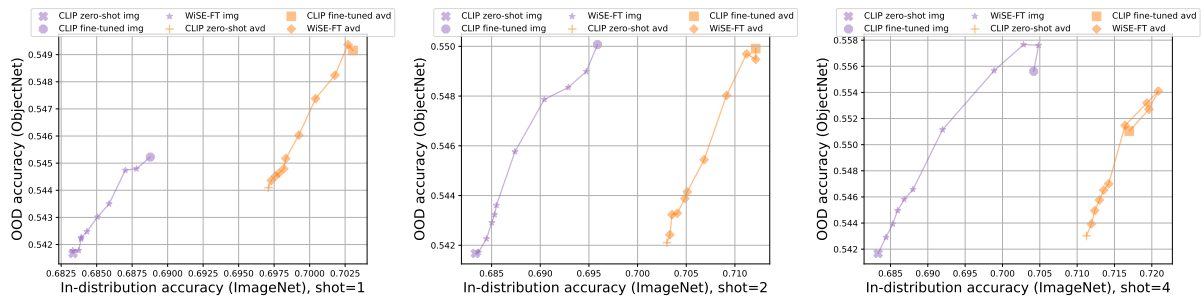


Figure 15: ID-OOD curves of WISE-FT vs WISE-SLR on ObjectNet. $k = 1, 2, 4$.

Shots		$k = 1$		$k = 2$		$k = 4$		$k = 8$		$k = 16$		$k = 32$	
α	Methods	LP	AVD	LP	AVD	LP	AVD	LP	AVD	LP	AVD	LP	AVD
	0.0000		68.78	69.53	68.78	69.53	68.78	69.53	68.78	69.53	68.78	69.53	68.78
0.0001		68.79	69.54	68.83	69.54	68.85	69.54	68.87	69.55	68.92	69.55	68.94	69.55
0.0002		68.81	69.54	68.88	69.55	68.91	69.55	68.93	69.56	69.02	69.56	69.07	69.56
0.0004		68.86	69.56	68.96	69.58	69.03	69.58	69.09	69.59	69.24	69.59	69.35	69.59
0.0008		68.94	69.59	69.14	69.63	69.26	69.64	69.40	69.64	69.65	69.66	69.84	69.68
0.0016		69.06	69.62	69.38	69.72	69.63	69.74	69.93	69.79	70.36	69.79	70.70	69.83
0.0032		69.22	69.72	69.73	69.86	70.17	69.93	70.73	70.00	71.40	70.07	72.01	70.08
0.0063		68.99	69.81	69.69	70.06	70.71	70.22	71.54	70.40	72.52	70.50	73.38	70.51
0.0126		67.31	69.83	68.04	70.33	70.35	70.75	71.65	71.09	73.10	71.25	74.22	71.27
0.0251		62.15	69.26	63.91	70.33	68.12	71.18	70.42	71.88	72.45	72.23	74.12	72.36
0.0501		53.51	66.75	57.69	69.30	64.35	71.17	68.18	72.37	71.10	73.08	73.30	73.44
0.1000		44.41	61.19	51.99	66.38	60.59	69.99	65.81	71.96	69.62	73.45	72.46	74.26
0.2000		37.91	53.68	47.94	62.06	57.59	67.75	64.13	70.95	68.60	73.09	71.83	74.34
0.3000		35.35	49.40	46.43	59.57	56.41	66.32	63.42	70.15	68.19	72.62	71.58	74.21
0.4000		34.05	46.60	45.63	57.93	55.83	65.43	63.06	69.52	67.99	72.22	71.44	74.06
0.5000		33.22	44.72	45.12	56.82	55.44	64.80	62.82	69.14	67.85	72.00	71.33	73.94
0.6000		32.67	43.44	44.79	55.98	55.18	64.30	62.66	68.89	67.75	71.81	71.27	73.85
0.7000		32.27	42.47	44.52	55.39	54.99	63.92	62.54	68.68	67.70	71.67	71.23	73.77
0.8000		31.96	41.71	44.31	54.87	54.85	63.62	62.45	68.51	67.62	71.57	71.20	73.73
0.9000		31.69	41.11	44.17	54.47	54.74	63.39	62.39	68.36	67.59	71.48	71.17	73.71
1.0000		31.51	40.56	44.06	54.16	54.66	63.19	62.33	68.23	67.55	71.40	71.15	73.67

Table 6: Accuracies on ImageNet with difference choices of α . We compare LP vs SLR-AVD.

Shots		$k = 1$		$k = 2$		$k = 4$		$k = 8$		$k = 16$		$k = 32$	
α	Methods	LP	AVD	LP	AVD	LP	AVD	LP	AVD	LP	AVD	LP	AVD
	0.0000		58.66	59.03	58.66	59.03	58.66	59.03	58.66	59.03	58.66	59.03	58.66
0.0001		58.67	59.03	58.68	59.03	58.69	59.04	58.70	59.04	58.70	59.04	58.71	59.04
0.0002		58.68	59.02	58.68	59.04	58.70	59.04	58.71	59.04	58.70	59.04	58.73	59.04
0.0004		58.69	59.03	58.70	59.04	58.71	59.04	58.73	59.03	58.75	59.05	58.81	59.05
0.0008		58.70	59.03	58.75	59.06	58.81	59.06	58.84	59.06	58.88	59.06	58.99	59.06
0.0016		58.72	59.06	58.81	59.08	58.90	59.09	59.03	59.11	59.07	59.08	59.23	59.11
0.0032		58.69	59.07	58.77	59.13	58.97	59.18	59.15	59.19	59.20	59.16	59.47	59.21
0.0063		58.30	59.10	58.27	59.14	58.79	59.23	58.89	59.31	58.98	59.28	59.40	59.37
0.0126		56.77	58.90	56.41	59.16	57.40	59.30	57.56	59.45	57.79	59.49	58.34	59.59
0.0251		52.55	58.09	51.93	58.70	54.30	59.14	54.81	59.38	55.47	59.55	56.28	59.78
0.0501		45.05	55.46	45.65	57.11	49.68	58.20	51.10	58.73	52.54	59.13	53.86	59.76
0.1000		36.63	50.25	39.71	53.88	45.30	56.12	47.77	57.21	50.03	58.05	51.87	59.25
0.2000		30.30	43.39	35.56	49.45	42.08	53.33	45.47	55.21	48.38	56.46	50.61	58.29
0.3000		27.83	39.70	33.94	47.00	40.79	51.76	44.55	54.02	47.73	55.60	50.12	57.70
0.4000		26.59	37.37	33.09	45.44	40.10	50.76	44.09	53.25	47.39	55.02	49.88	57.31
0.5000		25.82	35.84	32.57	44.43	39.67	50.12	43.79	52.74	47.18	54.63	49.71	57.04
0.6000		25.28	34.73	32.22	43.70	39.40	49.63	43.59	52.36	47.03	54.37	49.62	56.82
0.7000		24.87	33.94	31.99	43.16	39.18	49.25	43.45	52.07	46.92	54.16	49.55	56.67
0.8000		24.59	33.33	31.80	42.72	39.03	48.95	43.34	51.86	46.83	54.02	49.49	56.54
0.9000		24.36	32.85	31.65	42.38	38.91	48.71	43.26	51.67	46.77	53.88	49.44	56.45
1.0000		24.17	32.42	31.53	42.08	38.80	48.51	43.19	51.54	46.72	53.79	49.41	56.35

Table 7: Accuracies on ImageNet variations with difference choices of α . We compare LP vs SLR-AVD. The results are averaged over all 5 ImageNet variations.

Shot		$k = 1$		$k = 2$		$k = 4$	
α	Method	WISE-FT	WISE-SLR	WISE-FT	WISE-SLR	WISE-FT	WISE-SLR
	0.00		58.39	59.07	58.39	59.21	58.39
0.02		58.40	59.09	58.40	59.22	58.45	59.39
0.04		58.40	59.11	58.44	59.27	58.53	59.45
0.06		58.42	59.11	58.46	59.31	58.62	59.49
0.08		58.42	59.12	58.48	59.33	58.69	59.58
0.10		58.44	59.14	58.51	59.38	58.73	59.63
0.20		58.46	59.20	58.65	59.48	59.07	59.97
0.40		58.50	59.29	58.82	59.68	59.40	60.24
0.60		58.55	59.38	58.97	59.80	59.60	60.37
0.80		58.56	59.44	58.98	59.75	59.68	60.19
1.00		58.58	59.49	58.98	59.74	59.50	59.88

Table 8: Accuracies on ImageNet variations with difference choice of α . We compare WISE-FT to WISE-SLR. The results are averaged over 5 ImageNet variations.

Shot		$k = 1$		$k = 2$		$k = 4$	
α	Method	WISE-FT	WISE-SLR	WISE-FT	WISE-SLR	WISE-FT	WISE-SLR
	0.00	68.33	69.71	68.33	70.30	68.33	71.13
	0.02	68.33	69.73	68.37	70.33	68.44	71.19
	0.04	68.37	69.76	68.45	70.35	68.53	71.24
	0.06	68.39	69.78	68.50	70.41	68.60	71.30
	0.08	68.39	69.82	68.53	70.49	68.68	71.36
	0.10	68.43	69.83	68.55	70.51	68.80	71.42
	0.20	68.51	69.92	68.74	70.68	69.20	71.64
	0.40	68.59	70.04	69.04	70.91	69.89	71.93
	0.60	68.70	70.18	69.29	71.12	70.28	72.09
	0.80	68.78	70.27	69.47	71.21	70.48	71.96
	1.00	68.88	70.31	69.59	71.21	70.42	71.70

Table 9: Accuracies on ImageNet with difference choice of α . We compare WISE-FT to WISE-SLR.